

# Controlling noise with self-organized resetting

Felix J. Meigel<sup>1,2</sup> and Steffen Rulands<sup>1,2\*</sup>

<sup>1</sup>*Max Planck Institute for the Physics of Complex Systems,  
Noethnitzer Str. 38, 01187 Dresden, Germany and*

<sup>2</sup>*Ludwigs-Maximilians-Universität München, Arnold Sommerfeld Center  
for Theoretical Physics, Theresienstr. 37, 80333 München, Germany*

(Dated: September 23, 2024)

Biological systems often consist of a small number of constituents and are therefore inherently noisy. To function effectively, these systems must employ mechanisms to constrain the accumulation of noise. Such mechanisms have been extensively studied and comprise the constraint by external forces, nonlinear interactions, or the resetting of the system to a predefined state. Here, we propose a fourth paradigm for noise constraint: self-organized resetting, where the resetting rate and position emerge from self-organization through time-discrete interactions. We study general properties of self-organized resetting systems using the paradigmatic example of cooperative resetting, where random pairs of Brownian particles are reset to their respective average. We demonstrate that such systems undergo a delocalization phase transition, separating regimes of constrained and unconstrained noise accumulation. Additionally, we show that systems with self-organized resetting can adapt to external forces and optimize search behavior for reaching target values. Self-organized resetting has various applications in nature and technology, which we demonstrate in the context of sexual interactions in fungi and spatial dispersion in shared mobility services. This work opens routes into the application of self-organized resetting across various systems in biology and technology.

## INTRODUCTION

Many non-equilibrium systems, particularly in the context of biology, consist of a small number of constituents and are inherently noisy [1–7]. Such systems perform specific functions, such as sensing and signal processing in cells [8–10], or the coordination of animal movements in flocks and herds [11, 12]. Similarly, in technological applications, non-equilibrium systems are used in chemical reaction containers [13, 14], or to coordinate shared mobility solutions [15]. If unregulated, noise tends to accumulate over time such that the behavior of such systems becomes increasingly unpredictable. To perform a function, these systems must therefore employ mechanisms to constrain the accumulation of noise.

These mechanisms for controlling noise have been extensively studied across disciplines, such as in biological [16–18] and technological [19–21] contexts: First, noise can be constrained by external fields that restrict the time evolution of a stochastic system to a phase-space region centered around a stable attractor. Specifically, these external fields generate generalized forces that suppress small perturbations away from the attractor, continuously reducing noise within the system. For example, during embryonic development, the determination of cell identity is controlled by external morphogen gradients, leading to spatially separated domains in the embryo [8, 10, 22, 23]. In these systems, the coordination of constituents is regulated externally, without relying on interactions between the constituents.

In contrast to extrinsic forces, fluctuations can also be constrained intrinsically using self-organization: A stable steady state emerges from interactions between constituents if the strength of these interactions is significantly greater than the amplitude of the noise. Examples of the self-organized constraint of noise are abundant in nature, ranging from flocking phenomena in active matter systems [2, 11, 16] to genetic switches in cells [24–26].

Instead of the continuous suppression of fluctuations by external forces or self-organization, noise can also be controlled by resetting the constituents of a system to predefined states. In these systems, noise is controlled by time-discrete jumps that reset the system to a predefined state. These processes are commonly referred to as stochastic resetting. Because the state, to which the system is reset to, is extrinsically defined, we refer to these mechanisms as extrinsic resetting. Extrinsic resetting leads to the emergence of stationary distributions with finite variance [27, 28] such that dispersion and extreme fluctuations are constrained [29, 30]. Extrinsic resetting processes may include drift-diffusion dynamics [31–33], multiplicative diffusion [34–36], and space-dependent resetting rates and positions as well as non-ergodic stochastic dynamics [37–42]. Extrinsic resetting events are, for example, realized by the RNA-Polymerase where misaligned polymer ends are randomly cleaved [43] or employed in the context of biochemical systems to grant efficiency of reaction dynamics [14, 44–46].

Here, we investigate a fourth class of mechanisms for the constraint of fluctuations in which system

Figure 1.

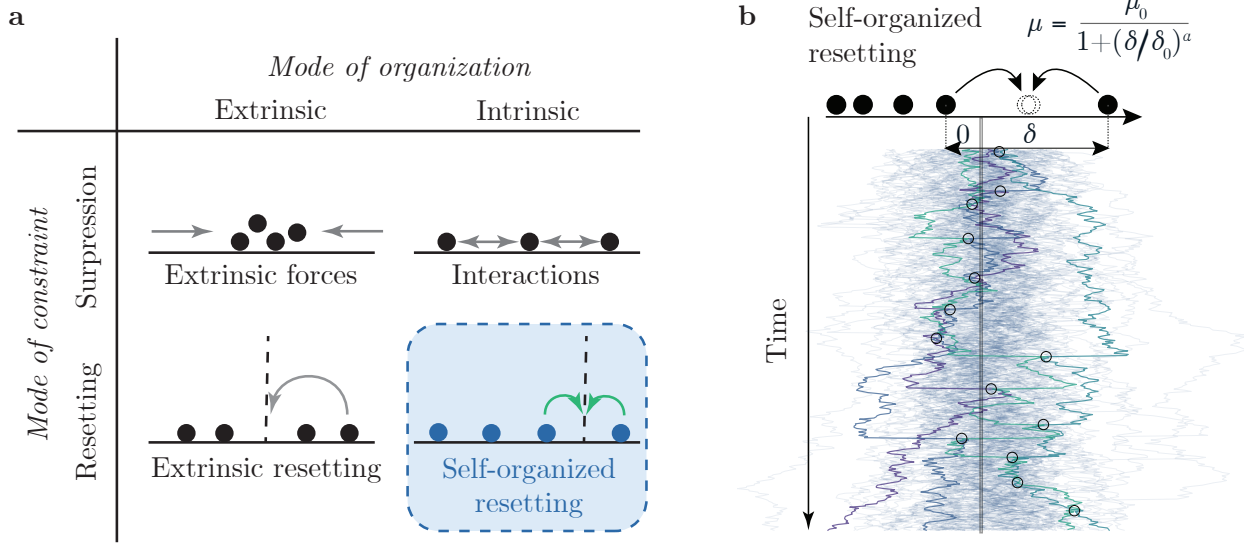


Figure 1. **a** Schematic illustrating different mechanisms that constrain the accumulation of noise. **b** Illustration of self-organized resetting: Exemplary trajectories obtained from agent-based simulations for cooperative resetting, where stochastic particles are randomly reset to their respective average. Each line represents the stochastic trajectory of a particle. Exemplary trajectories are highlighted by bold lines; resetting points are marked by circles.

constituents are reset to positions determined in a self-organized manner by time-discrete interactions (Fig. 1a). Examples of such dynamics are ubiquitous in nature and describe, for example, the averaging of molecular concentrations during the fusion and fission of intra-cellular organelles and chromatin-domain droplets [47–51], or the stem cell population dynamics during intestinal crypt fusion [52]. Further prominent examples include the genetic recombination dynamics during sexual reproduction [53, 54], or the mixing of populations in ecological systems, in origin-of-life scenarios, and genetic tracing experiments [55–58].

We illustrate the rich dynamic behavior inherent to self-organized resetting schemes by focusing on the paradigmatic example of *cooperative resetting*. This example involves a many-particle system driven by two dynamics: the accumulation of noise governed by a stochastic process for each constituent, and random events of pair-wise resetting to their respective average (Fig. 1b). We show that self-organized, cooperative resetting leads to a stationary state with bounded variance if interactions are sufficiently long-ranged. In analogy to condensed-matter physics [59], we refer to the boundedness of the variance as *localization*. As interactions become increasingly short-ranged, self-organized resetting undergoes a delocalization transition. In the relevant case that interactions between particles decay

quadratically, we identify a second-order phase transition depending on the particle density. As a consequence of localization, stochastic resetting enhances the search behavior of the stochastic process, resulting in a decreased time for constituents to reach a target state compared to Brownian particles. We exemplify the generality of our findings by using the framework of self-organized, cooperative resetting to explain the fitness advantage of sexual interaction in fungi and to demonstrate its applicability in designing organization strategies in shared mobility services.

## RESULTS

### Definition of cooperative resetting

To investigate general properties of self-organized resetting systems, we focus on a simple, but paradigmatic model that comprises  $N$  particles described by their positions  $X_i$  in one spatial dimension. These particles undergo Brownian motion with a diffusion constant  $D$ . Pairs of particles can interact with a rate  $\mu$  that depends on the distance  $\delta = |X_i - X_j|$  between the particles. Upon such an interaction, the positions of both particles are set to their respective mean position,  $(X_i + X_j)/2$ . Beyond a characteristic length scale  $\delta_0$ , these interac-

tions decay algebraically with an exponent  $\alpha$ ,

$$\mu(\delta) = \frac{\mu_0}{1 + (\delta/\delta_0)^\alpha}. \quad (1)$$

As we will discuss below, this choice of kernel allows us to draw conclusions about general interactions.

To describe the collective dynamics of this system, we study the single-particle probability density,  $p(x, t)dx$ , of finding a particle between positions  $x$  and  $x + dx$ . The time evolution of  $p(x, t)$  is governed by two processes: the effect of Brownian motion, which depends on the single-particle density  $p(x, t)$ , and the pair-wise resetting, which depends on the two-particle density  $p_2(x, x', t)$ . Using an operator notation, the time evolution of  $p(x, t)$  follows an equation of the form

$$\partial_t p(x, t) = \hat{\mathcal{L}}[p(x, t)] + \hat{\mathcal{R}}[p_2(x, x', t)]. \quad (2)$$

We give the definitions of the operators  $\hat{\mathcal{L}}$  and  $\hat{\mathcal{R}}$  in Appendix A.

We now ask under which conditions cooperative resetting can constrain the accumulation of fluctuations stemming from Brownian motion. Fluctuations are constrained if Eq. (2) admits a steady state with finite variance, i.e. it exhibits localization. We first note that cooperative resetting leads to a displacement of particles with an associated flux  $-\partial_x \hat{J}_{\mathcal{R}} = \hat{\mathcal{R}}$ . In the steady state, this flux must be balanced with the flux associated with Brownian motion,  $-\partial_x \hat{J}_{\mathcal{L}} = \hat{\mathcal{L}}$ , Appendix B,

$$\hat{J}_{\mathcal{R}}[p_2(x, x', t)] = -\hat{J}_{\mathcal{L}}[p(x, t)]. \quad (3)$$

To assess if cooperative resetting admits for localized states, we test for the existence of a steady-state distribution that fulfills flux balance and is normalizable. To obtain a closed form in terms of the single-particle density,  $p(x, t)$ , we employ a mean-field approximation,  $p_2(x, x', t) = p(x, t)p(x', t)$ . We further approximate the left-hand side of Eq. (3) in the limit  $|x| \rightarrow \infty$  to first order in  $1/|x|$  (see Appendix C for the detailed derivation). With this, we obtain for  $\delta$ -distributed initial conditions at  $x_0 = 0$  a flux-balance condition for localization in terms of the steady-state probability distribution  $p_s(x)$ ,

$$\varrho p_s(\chi) \left| \frac{p_s(\chi)}{p'_s(\chi)} \right| |\chi|^{-\alpha} \stackrel{!}{=} p'_s(\chi). \quad (4)$$

Here, we defined non-dimensional positions by rescaling lengths by the characteristic length scale of interactions  $\chi = x/\delta_0$ . We defined a non-dimensional parameter  $\varrho = 2N\delta_0^2\mu_0/D$  which has the interpretation of a rescaled average particle density.  $p'_s(\chi)$  denotes the derivative of  $p_s(\chi)$  with respect to  $\chi$ .

## Conditions for localization

In Eq. (4), we rephrased the resetting flux in a way that admits an intuitive interpretation. The first factor in the resetting flux,  $p_s(\chi)$ , is proportional to the number of particles contributing to the flux at position  $\chi$ , the second factor gives the effective length of jumps due to resetting, and the third factor is the first-order approximation of the resetting rate of Eq. (1), Fig. 2a. Notably, Eq. (4) is a first-order non-linear differential equation, which admits analytical solutions. Solving for  $p_s(\chi)$  for given values of  $\alpha$  and  $\varrho$  then allows us to determine under which conditions cooperative resetting admits for localized solutions and to calculate the functional form of  $p_s(\chi)$  in the limit  $|\chi| \rightarrow \infty$ .

Using Eq. (4), we now investigate localization conditions for different values of  $\alpha$  and  $\varrho$ . For  $\alpha = 0$ , particles undergo pair-wise resetting independent of their distance. In this case, Eq. (4) admits stationary solutions and the cooperative resetting process exhibits localized states. Specifically, the stationary solutions asymptotically approach an exponential form,  $p_s(\chi) \sim e^{-\sqrt{\varrho}|\chi|}$ , for  $|\chi| \rightarrow \infty$ . Notably, in this case, cooperative resetting exhibits localization for all values of  $\varrho$ . We corroborated this result and all further results by agent-based simulations of Brownian motion and the resetting processes defined above.

The stationary solution of the cooperative resetting process has the same asymptotic form as that of the extrinsic resetting process, where the particles are reset with a fixed rate to their initial position  $\chi_0$  [60] if the rate of extrinsic resetting is set to  $\mu_{\text{ext}} = \mu_0 N$  (Fig. 2b). However, because extrinsic resetting processes yield a higher probability for a particle to be close to the initial position  $\chi_0$ , the probability for a particle to be found at a position in the tail of the probability density function is increased by a constant factor for cooperative resetting.

If resetting is distance-dependent,  $\alpha > 0$ , the resetting rate depends on the local particle density. In this case, Eq. (4) yields for  $\alpha \neq 2$  and in the limit  $|\chi| \rightarrow \infty$  stationary solutions of exponential form,

$$p_s(\chi) \sim \exp \left[ -\sqrt{\varrho}|\chi|^{1-\alpha/2}/(1-\alpha/2) \right]. \quad (5)$$

These solutions have decaying tails for  $\alpha < 2$ . In this case, resetting interactions are sufficiently long-ranged such that a balance between Brownian motion and resetting gives rise to a localized steady state (Fig. 2c). For  $\alpha > 2$  the tails do not decay such that Eq. (4) does not admit steady-state solutions which are normalizable probability density functions. In this case, the stochastic dynamics is dominated by Brownian motion.

Figure 2.

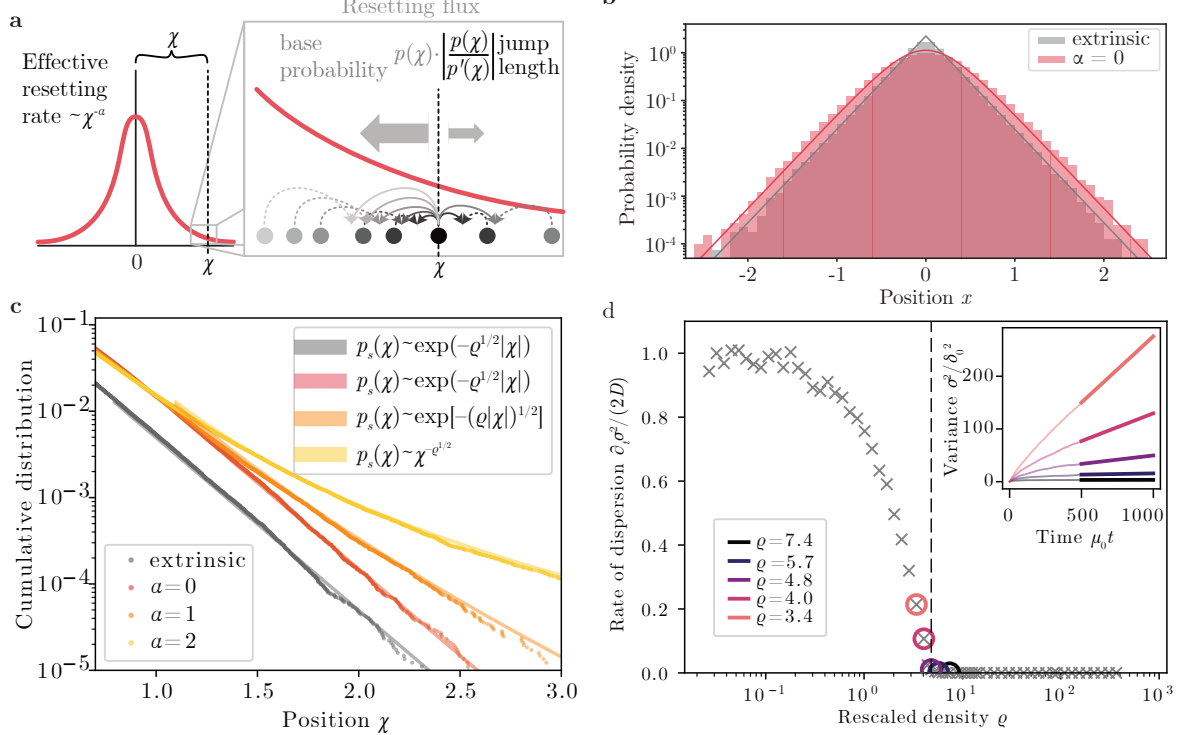


Figure 2. **a** Interpretation of the approximated resetting flux in Eq. (4) as the product of an effective resetting rate, the density of particles contributing to the flux, and the effective jump length of resetting events. **b, c** Agent-based simulations (dots) of  $N = 2 \times 10^5$  particles for cooperative and extrinsic resetting with  $\varrho = 21$ . **b** Histograms for cooperative and extrinsic resetting which both decay exponentially for  $\alpha = 0$ . **c** The cumulative distribution is defined as  $\int_x^\infty p_s(x) dx$ . Lines represent the predicted functional dependencies from Eq. (5). The offset of the theoretical prediction is fitted to the simulation data. **d** For  $\alpha = 2$  we find a phase transition dependent on the particle density. The inset shows the increase in the variance over time. For particles performing Brownian motion, the variance increases as  $\sigma^2 = 2Dt$ . The slopes of the increase of the variance in the long-time limit (thick lines in inlay) define an effective order parameter, which is shown in the main plot. If the rescaled density is below a critical density,  $\varrho < \varrho_c$ , the probability density function delocalizes. Crosses depict results from agent-based simulations of  $N = 2 \times 10^5$  particles. Circles depict values of  $\varrho$  that are represented in the inlay with matched color. The dashed line is the critical density  $\sqrt{\varrho_c} = 2.3$  estimated analytically (Appendix D).

Therefore, cooperative resetting exhibits a delocalization transition for increasing values of  $\alpha$ : Localization occurs for all positive values of the rescaled density  $\varrho$  for  $\alpha < 2$  and no localization occurs for  $\alpha > 2$ . As a consequence, any interaction kernel decaying faster than  $\mu(\delta) \sim \delta^{-2}$  in the limit  $\delta \rightarrow \infty$  does not admit for localization. This in particular includes interaction kernels with an exponential decay.

Interactions decaying with an exponent of  $\alpha = 2$  are ubiquitous in nature [61]. They also form a special case in the cooperative resetting process as the exponent Eq. (5) diverges. In this case, the steady-state solution of Eq. (4) decays algebraically,  $p_s(\chi) \sim \chi^{-\sqrt{\varrho}}$ , which we also find in numerical simulations (Fig. 2b). The probability density function is not normalizable for  $\sqrt{\varrho} > 1$ . This suggests that for  $\alpha = 2$  the cooperative resetting

process undergoes a delocalization transition with decreasing values of the rescaled density,  $\varrho$ . For  $\varrho \rightarrow 0$  the typical distance between particles is large such that the overall rate of resetting is small. This regime is therefore dominated by diffusion. For  $\varrho \rightarrow \infty$ , resetting processes dominate and we find that the probability density localizes (Fig. 2d). While the normalization condition gives a rough estimate for the critical value of the rescaled density of  $\varrho_c \approx 1$ , an analysis of Eq. (4) including higher orders yields an improved approximation of  $\sqrt{\varrho_c} \approx 2.3$ , see Appendix D. In general, these results imply that with an increasing number of particles,  $N$ , or a decreasing diffusion constant,  $D$ , cooperative resetting with quadratically decaying interactions exhibits a localization phase transition.

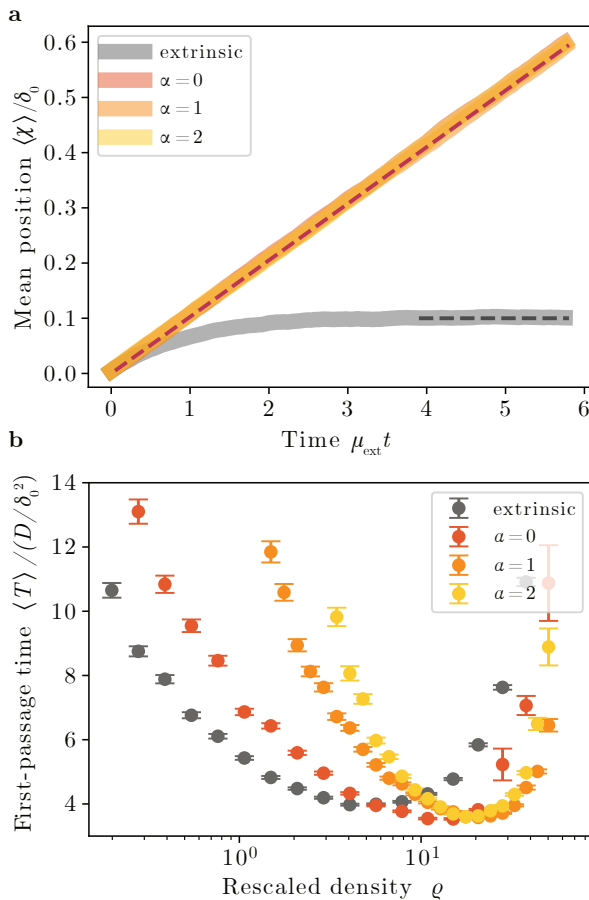
**Figure 3.**

Figure 3. **a** Localised states emerging from cooperative resetting differ qualitatively from localized states emerging from extrinsic resetting in their response to external forces and search behavior. Agent-based simulations ( $\varrho = 21$ ) for cooperative resetting and extrinsic resetting which are subject to a fixed drift  $v\delta_0/\mu_{\text{ext}} = 0.1$ . For extrinsic resetting, the localized states remain close to the resetting position  $\chi_0$ , while for cooperative resetting the localized state translocates with the drift  $v$ . **b** The minimal mean first passage time for a marked particle in an ensemble of 200 particles to reach a target at a distance  $l = 0.4$  is compared for intrinsic and cooperative resetting as  $\varrho$  is varied through  $\mu_0$ . The minimal mean first passage time is reduced for the cooperative resetting scheme. Averages are taken over  $n = 5000$  simulations and error bars represent the standard error of the mean.

### Adaptation and search behavior

Having studied the steady-state behavior of the cooperative resetting process, we now ask how cooperative resetting systems respond to extrinsic forces. To this end, we apply a constant force  $F$  and study the response to it in the cooperative resetting model. We

compared our results to the extrinsic resetting model. In the over-damped limit, the constant force gives rise to a constant velocity of particles,  $v$ , which is proportional to  $F$ . For the extrinsic resetting scheme the localized state remains close to  $\chi_0$  and assumes a skewed distribution. The mean position takes a constant value that deviates from the resetting position,  $\langle \chi \rangle - \chi_0 = v/\mu_{\text{ext}}$  [60]. For the cooperative resetting scheme, the extrinsic force yields an additional drift flux of the form  $\hat{J}_{\mathcal{F}} = vp(\chi, t)$  in Eq. (3). Making the Galilean transformation  $\chi' = \chi - vt$  this flux vanishes. For cooperative resetting, the localized states remain symmetric and we instead find that the system responds with a translocation with constant velocity to the extrinsic force (Fig. 3a). Therefore, cooperative resetting systems can adapt to extrinsic forces while at the same time constraining intrinsic noise.

Stochastic resetting processes have been intensively studied in the context of search problems, in which one is interested in the time a particle takes to reach a given target position for the first time. Extrinsic stochastic resetting processes have the counter-intuitive property that they exhibit lower mean first-passage times compared to pure Brownian motion [27, 60]. In extrinsic resetting, an optimal resetting rate minimizes first-passage time for any target distance  $l = \chi^* - \chi_0$ : high resetting rates lead to frequent resets, even for particles close to targets, while low resetting rates result in infrequent resets, allowing the particle to wander off in the wrong direction.

To investigate the search dynamics in cooperative resetting systems, we study the first-passage time of a single, randomly chosen particle. We numerically find that if the cooperative resetting dynamics admits for a localized state, there is an optimal density  $\varrho^*$  which minimizes the first-passage time for a given target distance,  $l$ , (Fig. 3b). The search is generally improved for cooperative resetting as the minimal mean first-passage time is lower compared to extrinsic resetting. This is intuitive, as in cooperative resetting, the reduced probability of the particle being close to the initial position  $\chi_0$  (Fig. 2b) leads to an increased flux away from  $\chi_0$ . This reduces the impact of retracting steps close to the target. A similar effect is achieved in models comprising a non-resetting window around  $\chi_0$ , which has been shown to reduce the minimal first-passage time for extrinsic resetting [37]. Next, we apply our theoretical findings to the inhibition of fluctuations in biological and technical systems.



Figure 4.

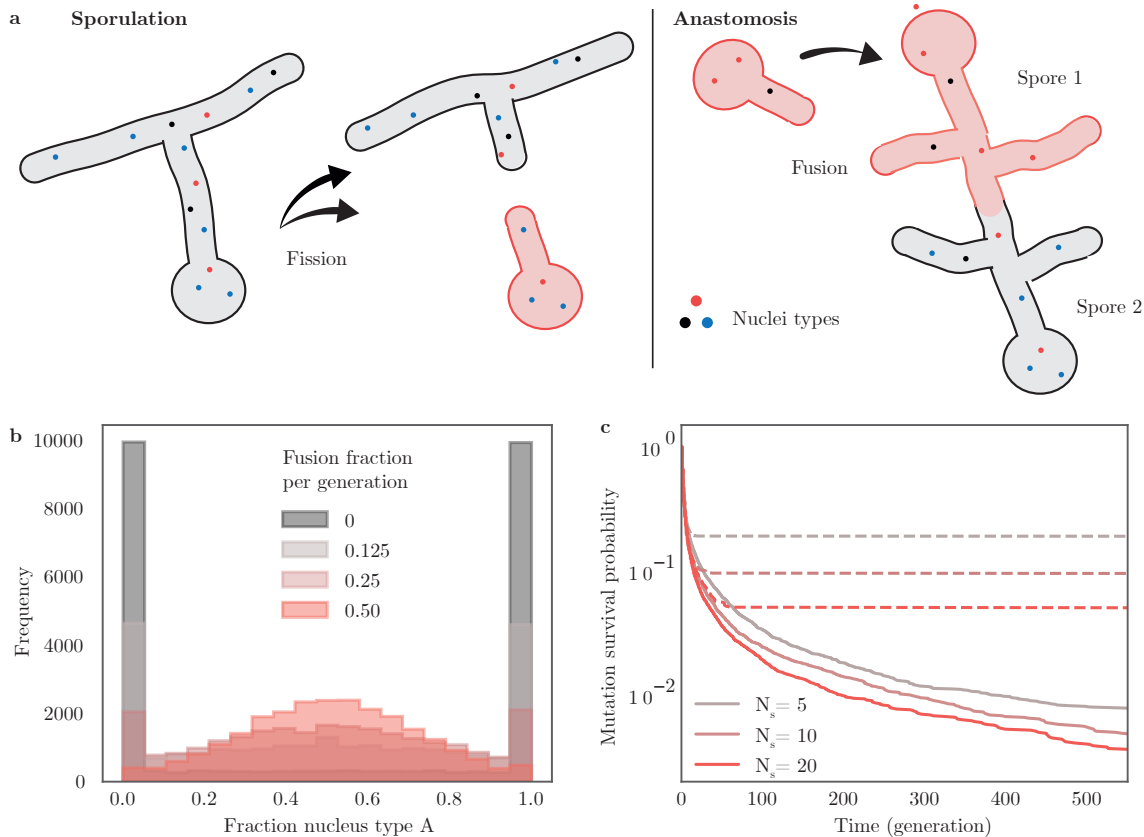


Figure 4. Fungi constrain genetic variability by self-organized resetting through anastomosis. **a** Multi-nucleated fungi undergo cycles of sporulation and anastomosis, as the hyphae of different fungi fuse and allow the exchange of nuclei. Fungi spores carry only a subset of nuclei and sporulation acts effectively as a fission event. Iterative fusion and fission implement pairwise cooperative resetting. **b** Stochastic simulations of fungal populations demonstrate hyphal fusion to preserve genetic heterogeneity of neutral genes by self-organized resetting. Genetic heterogeneity is quantified in a population snapshot after 25 generations. Different colors represent different probabilities for fungi to undergo anastomosis with a different fungus after sporulation and subsequent germination. The spore size is  $N_s = 20$ . **c** Simulations show an increased probability for fixation of neutral mutations in the absence of anastomosis (dotted lines). Fungi undergo anastomosis with a probability of 25% after germination (bold lines). Different colors indicate different effective spore sizes in terms of the number of enclosed nuclei.

### Sexual recombination in fungi

We illustrate the application of self-organized resetting through the paradigmatic biological example of sexual reproduction. Specifically, we focus on the sexual interactions among filamentous fungi: Coenocytic fungal species, such as *Zygomycota* and *Glomeromycota*, are multinucleated organisms containing nuclei with diverse genetic identities [62–66]. These filamentous fungal species form networks of interconnected hyphae with nuclei that freely move in the cytoplasm. The nuclei in a fungus replicate asexually through division during colony growth. A fungal organism as a whole reproduces via sporulation, during which a subset of

nuclei is encapsulated and emitted from the fungus. Upon germination, these spores establish new fungal colonies. Hyphae from different fungi can fuse upon contact (anastomosis), facilitating the exchange of nuclei between the two fungi (Fig. 4a). The genetic diversity of nuclei is hypothesized to grant the ability of fungi to rapidly evolve in changing environments [62].

The number of nuclei per spore is relatively small compared to the total number of nuclei in a fungal network and varies from a few tens to thousands of nuclei in a single spore [63]. On the level of an isolated fungus, the homogenous states are absorbing states, where a single nuclei genotype can achieve fixation. One would therefore expect genotypes within a fungus to go ex-

tinct on the timescale of a few fungal generations. In contrast, hyphal fusion leads to an effective averaging of the fractions of different genotypic nuclei among fungi. This is a manifestation of cooperative resetting. We therefore predict that the localization of the probability density function of nuclear genotype fractions could lead to long-term stabilization of genetic diversity.

To test this, we performed stochastic simulations of the numbers  $n_i$  of nuclei with a genotype  $i$  in a population of  $N = 2.5 \times 10^4$  fungi, accounting for fungal growth with nuclei replication dynamics as well as sporulation, and anastomosis. Here, a cycle of germination followed by sporulation defines a unit of time which we refer to as a generation. In a minimal model, we consider two genotypes with equal fitness, a constant generation progression time, and restrict hyphal fusion to fungi colonies in the same generation. We set our model parameter based on physiological estimates: In agreement with [63], we varied the number of nuclei of spores between  $N_s = 5$  and 20. We fixed the number of fungi by setting the number of germinating spores to one per colony, considering that the successful germination rate of fungi in wildlife conditions is significantly below rates measured in the laboratory [64]. We varied the number of successful anastomosis events between germinated spores in the range of 12% to 50%, [62, 64, 66]. After germination, our model comprises a growth phase of 7 nuclear divisions, where the set of newly formed nuclei stems from a one-step Moran process. For sporulation, a random subset of nuclei is picked from the fungal colony. An equal number of nuclei of both genotypes was set as an initial condition.

Our simulations show that in the absence of fungal fusion, genetic diversity is largely lost over the course of the simulation (25 generations), as more than 70% of colonies exhibit fixation of one type of nuclei. Sexual recombination by hyphal fusion leads to a localization of the fraction of genotypes at 50% (Fig. 4b). While cooperative resetting facilitates the maintenance of existing genetic diversity, it also leads to the rapid extinction of new mutations (Fig. 4c). Significantly, our qualitative findings are robust to changes in the parameter choice, as long as the number of nuclei in a spore is much smaller than the number of nuclei in the fungal colony.

### Localization of shared mobility devices

As an illustration of utilizing cooperative resetting in a technical application, we study the dispersion of vehicles in shared mobility services. Users of these services book vehicles for individual rides, where they pick up

the shared vehicle close to their starting position and drop it off at their destination. The major challenge for companies offering shared mobility services is providing vehicles at locations with a high demand [67]. At the same time, the randomness in pick-up and drop-off gives rise to a spatial dispersion of vehicles over time, [15], resulting in an increase of the average distance between vehicles, which consequently implies a reduction in the local availability of vehicles. Thus, mechanisms that constrain the spatial dispersion of vehicles are of central interest to companies providing shared mobility services.

Next, we exemplify that cooperative pair-wise resetting is a possible viable mechanism to implement a self-organized resetting scheme for shared mobility services. We simulate simple pick-up and drop-off dynamics of the shared vehicles as a random walk on the street network of Munich, which we obtained from Open Street Map [68] and in which intersections define nodes. We set the length of a random ride to  $N_{\text{length}} = 10$  streets being traversed. We compared three models: First, an implementation without resetting in which vehicles may freely disperse; Second, a model with extrinsic resetting, in which vehicles are reset to the initial starting point. This mimics services in which vehicles are collected and collectively dropped off at central locations. Thirdly, we also study a model, in which vehicles are reset pair-wise through the coordinated interactions of users. In the simulations, this means that we pick two random scooters and reset them to the junction closest to their spatial average.

Expectedly, without resetting, vehicles disperse unconstrained, but subdiffusively while extrinsic or cooperative resetting constrains the dispersion of vehicles to a defined area (Fig. 5a, b). We next study the effect of a change in customer preferences by assuming that, on average, one in 100 rides has a specific destination on the map. Because cooperative resetting allows for the simultaneous constraint of noise and an adaption to extrinsic forces (Fig. 3a) we expect that a cooperative resetting scheme will adapt to changes in customer preferences while restricting the dispersion of vehicles. With extrinsic resetting of the vehicles, the probability density function remains localized around the resetting position (Fig. 5b) while for cooperative resetting the mode of the probability density function adapts to the bias in the drop-off locations (Fig. 5c).

## DISCUSSION

With self-organized resetting, we have studied a paradigm for the constraint of fluctuations in stochas-

Figure 5.



Figure 5. Cooperative resetting suppresses the spatial dispersion of vehicles while allowing for the adaptation of trends. **a** Simulation snapshot of the spreading dynamics of a vehicle cohort ( $N = 100$ ) in the absence of resetting (red) and while undergoing cooperative resetting (blue) after 100 random rides. Vehicles perform random walks on the street network of Munich. Each ride has a length of 10 steps and 10% of rides were followed by a cooperative resetting event. The initial position (central station of Munich) is marked by an orange star. The inset shows the spatial variance of the vehicle cohort over time. In the presence of cooperative resetting, the spatial variance is bounded (localization). **b** Simulation snapshot of a scooter cohort subject to an extrinsic resetting scheme to the initial position (orange star) after 400 rides. Preferential rides (1% of the rides) to the quarter 'Au-Haidhausen' (orange outline) do not lead to re-localization in this quarter. **c** Same as b, but for cooperative resetting (10% of rides). An overlay of different time points (color-coded) demonstrates the temporal adaptation as the spatially localized cohort shifts to the quarter Au-Haidhausen.

tic systems. We showed that self-organized resetting allows for the suppression of the accumulation of noise in stochastic many-particle systems. This mechanism is conceptually different compared to other mechanisms for the constraint of noise using external signals, or self-organization schemes that demand the continuous suppression of noise. We exemplify the concept of self-organized resetting by focusing on the mechanism of cooperative resetting, where random pairs of constituents reset to their respective average. We showed that such a self-organized resetting scheme gives rise to localization phase transitions as a function of the spatial decay of resetting interactions and the particle density. Cooperative resetting systems respond differently to external forces if localization occurs and show improved search behavior compared to extrinsic resetting. Our work shows that the localization and search properties of extrinsic resetting schemes can be obtained in a self-organized manner without the need for extrinsic control.

While studying the localization phase transition in a simple cooperative resetting scheme for Brownian noise admits for analytical solutions, we expect our results to be qualitatively valid also for multiplicative and colored noise. Making the ansatz of the resetting flux balancing a flux attributable to the spreading dynamics, our calculations are generalizable to any stochastic system that is describable in terms of a moment expansion to

second order. Additionally, our approach can be extended to include additional extrinsic force fields or to higher dimensions.

We have demonstrated two applications of self-organized resetting: sexual interactions in filamentous fungi and the spreading dynamics of shared mobility solutions. While we here focused on two specific examples, we expect that self-organized resetting is a general and abundant mechanism for constraining fluctuations. Further applications for self-organized resetting range from intracellular signaling pathways on fusion and fission organelles, stem-cell dynamics in fusing intestinal crypts, or - as an economical application - the redistribution of wealth through altruistic donations in economic systems [69, 70]. We think that self-organized resetting is a general mechanism to control the accumulation of noise in stochastic many-constituent systems.

We thank M. Ciarchi, R. Mukhamadiarov, and F. Jülicher for their helpful feedback and the entire Rulands group for critical discussions. This project has received funding from the European Research Council (ERC) under the European Union's Horizon 2020 research and innovation program (grant agreement no. 950349).



- \* rulands@lmu.de
- [1] Rasmussen, S. *et al.* Transitions from Nonliving to Living Matter. *Science* **303**, 963–965 (2004). URL <https://www.science.org/doi/abs/10.1126/science.1093669>. Publisher: American Association for the Advancement of Science.
  - [2] Vicsek, T., Czirók, A., Ben-Jacob, E., Cohen, I. & Shochet, O. Novel Type of Phase Transition in a System of Self-Driven Particles. *Phys. Rev. Lett.* **75**, 1226–1229 (1995). URL <https://link.aps.org/doi/10.1103/PhysRevLett.75.1226>. Publisher: American Physical Society.
  - [3] Wong, G. C. L. *et al.* Roadmap on emerging concepts in the physical biology of bacterial biofilms: from surface sensing to community formation. *Phys. Biol.* **18**, 051501 (2021). URL <https://dx.doi.org/10.1088/1478-3975/abcd0e>. Publisher: IOP Publishing.
  - [4] Bäuerle, T., Fischer, A., Speck, T. & Bechinger, C. Self-organization of active particles by quorum sensing rules. *Nat Commun* **9**, 3232 (2018). URL <https://www.nature.com/articles/s41467-018-05675-7>. Publisher: Nature Publishing Group.
  - [5] Swain, P. S., Elowitz, M. B. & Siggia, E. D. Intrinsic and extrinsic contributions to stochasticity in gene expression. *Proc. Natl. Acad. Sci. U.S.A.* **99**, 12795–12800 (2002). URL <https://www.pnas.org/doi/abs/10.1073/pnas.162041399>.
  - [6] Süel, G. M., Kulkarni, R. P., Dworkin, J., Garcia-Ojalvo, J. & Elowitz, M. B. Tunability and Noise Dependence in Differentiation Dynamics. *Science* **315**, 1716–1719 (2007). URL <https://www.science.org/doi/full/10.1126/science.1137455>.
  - [7] Lestas, I., Vinnicombe, G. & Paulsson, J. Fundamental limits on the suppression of molecular fluctuations. *Nature* **467**, 174–178 (2010). URL <https://www.nature.com/articles/nature09333>.
  - [8] Gregor, T., Tank, D. W., Wieschaus, E. F. & Bialek, W. Probing the Limits to Positional Information. *Cell* **130**, 153–164 (2007). URL [https://www.cell.com/cell/abstract/S0092-8674\(07\)00662-9](https://www.cell.com/cell/abstract/S0092-8674(07)00662-9). Publisher: Elsevier.
  - [9] Petkova, M. D., Tkačik, G., Bialek, W., Wieschaus, E. F. & Gregor, T. Optimal decoding of cellular identities in a genetic network. *Cell* **176**, 844–855 (2019). URL [https://www.cell.com/cell/pdf/S0092-8674\(19\)30040-6.pdf](https://www.cell.com/cell/pdf/S0092-8674(19)30040-6.pdf). Publisher: Elsevier.
  - [10] Kicheva, A., Bollenbach, T., Wartlick, O., Jülicher, F. & Gonzalez-Gaitan, M. Investigating the principles of morphogen gradient formation: from tissues to cells. *Current Opinion in Genetics & Development* **22**, 527–532 (2012). URL <https://www.sciencedirect.com/science/article/pii/S0959437X12000998>.
  - [11] Bialek, W. *et al.* Social interactions dominate speed control in poising natural flocks near criticality. *Proceedings of the National Academy of Sciences* **111**, 7212–7217 (2014). URL <https://www.pnas.org/doi/full/10.1073/pnas.1324045111>. Publisher: Proceedings of the National Academy of Sciences.
  - [12] Demšar, J., Hemelrijk, C. K., Hildenbrandt, H. & Bajec, I. L. Simulating predator attacks on schools: Evolving composite tactics. *Ecological Modelling* **304**, 22–33 (2015). URL <https://www.sciencedirect.com/science/article/pii/S0304380015000745>.
  - [13] Meigel, F. J., Darwent, T., Bastin, L., Goehring, L. & Alim, K. Dispersive transport dynamics in porous media emerge from local correlations. *Nat Commun* **13**, 5885 (2022). URL <https://www.nature.com/articles/s41467-022-33485-5>. Publisher: Nature Publishing Group.
  - [14] Reuveni, S., Urbakh, M. & Klafter, J. Role of substrate unbinding in Michaelis–Menten enzymatic reactions. *Proc. Natl. Acad. Sci. U.S.A.* **111**, 4391–4396 (2014). URL <https://www.pnas.org/doi/full/10.1073/pnas.1318122111>.
  - [15] McKenzie, G. Urban mobility in the sharing economy: A spatiotemporal comparison of shared mobility services. *Computers, Environment and Urban Systems* **79**, 101418 (2020). URL <https://www.sciencedirect.com/science/article/pii/S0198971519303060>.
  - [16] Hueschen, C. L., Dunn, A. R. & Phillips, R. Wildebeest herds on rolling hills: Flocking on arbitrary curved surfaces. *Phys. Rev. E* **108**, 024610 (2023). URL <https://link.aps.org/doi/10.1103/PhysRevE.108.024610>. Publisher: American Physical Society.
  - [17] Skinner, D. J., Jeckel, H., Martin, A. C., Drescher, K. & Dunkel, J. Topological packing statistics of living and nonliving matter. *Science Advances* **9**, eadg1261 (2023). URL <https://www.science.org/doi/10.1126/sciadv.adg1261>. Publisher: American Association for the Advancement of Science.
  - [18] Hoehn, S. S., Haas, P. A., Honerkamp-Smith, A. R. & Goldstein, R. E. Mechanics of Cell Sheet Folding–Embryonic Inversion in the Green Algae *Volvox*. *Biophysical Journal* **116**, 19a (2019). URL [https://www.cell.com/biophysj/pdf/S0006-3495\(18\)31408-5.pdf](https://www.cell.com/biophysj/pdf/S0006-3495(18)31408-5.pdf). Publisher: Elsevier.
  - [19] Cheng, C.-T., Tse, C. K. & Lau, F. C. M. A Clustering Algorithm for Wireless Sensor Networks Based on Social Insect Colonies. *IEEE Sensors Journal* **11**, 711–721 (2011). URL <https://ieeexplore.ieee.org/abstract/document/5582136>. Conference Name: IEEE Sensors Journal.
  - [20] Cremaldi, J. C. & Bhushan, B. Bioinspired self-healing materials: lessons from nature. *Beilstein J. Nanotechnol.* **9**, 907–935 (2018). URL <https://www.beilstein-journals.org/bjnano/articles/9/85>. Publisher: Beilstein-Institut.
  - [21] Torres, S. Swarm Theory Applied To Air Traffic Flow Management. *Procedia Computer Science* **12**, 463–470 (2012). URL <https://www.sciencedirect.com/science/article/pii/S1877050912006965>.
  - [22] Rulands, S., Klünder, B. & Frey, E. Stability of Localized Wave Fronts in Bistable Systems. *Phys. Rev. Lett.* **110**, 038102 (2013). URL <https://link.aps.org/doi/10.1103/PhysRevLett.110.038102>. Publisher: American Physical Society.
  - [23] Tkačik, G., Callan, C. G. & Bialek, W. Information flow and optimization in transcriptional regulation. *Proceedings of the National Academy of Sciences* **105**, 12265–

- 12270 (2008). URL <https://www.pnas.org/doi/abs/10.1073/pnas.0806077105>. Publisher: Proceedings of the National Academy of Sciences.
- [24] Gardner, T. S., Cantor, C. R. & Collins, J. J. Construction of a genetic toggle switch in *Escherichia coli*. *Nature* **403**, 339–342 (2000). URL <https://www.nature.com/articles/35002131>. Publisher: Nature Publishing Group.
- [25] Ferrell, J. E. & Machleder, E. M. The Biochemical Basis of an All-or-None Cell Fate Switch in *Xenopus* Oocytes. *Science* **280**, 895–898 (1998). URL <https://www.science.org/doi/10.1126/science.280.5365.895>. Publisher: American Association for the Advancement of Science.
- [26] Lebar, T. *et al.* A bistable genetic switch based on designable DNA-binding domains. *Nat Commun* **5**, 5007 (2014). URL <https://www.nature.com/articles/ncomms6007>. Publisher: Nature Publishing Group.
- [27] Evans, M. R. & Majumdar, S. N. Diffusion with Stochastic Resetting. *Phys. Rev. Lett.* **106**, 160601 (2011). URL <https://link.aps.org/doi/10.1103/PhysRevLett.106.160601>.
- [28] Manrubia, S. C. & Zanette, D. H. Stochastic multiplicative processes with reset events. *Phys. Rev. E* **59**, 4945–4948 (1999). URL <https://link.aps.org/doi/10.1103/PhysRevE.59.4945>.
- [29] Evans, M. R. & Majumdar, S. N. Diffusion with optimal resetting. *J. Phys. A: Math. Theor.* **44**, 435001 (2011). URL <https://dx.doi.org/10.1088/1751-8113/44/43/435001>.
- [30] Montero, M. & Villarroel, J. Monotonic continuous-time random walks with drift and stochastic reset events. *Phys. Rev. E* **87**, 012116 (2013). URL <https://link.aps.org/doi/10.1103/PhysRevE.87.012116>.
- [31] Ray, S., Mondal, D. & Reuveni, S. Péclet number governs transition to acceleratory restart in drift-diffusion. *J. Phys. A: Math. Theor.* **52**, 255002 (2019). URL <https://dx.doi.org/10.1088/1751-8121/ab1fcc>.
- [32] Ray, S. & Reuveni, S. Diffusion with resetting in a logarithmic potential. *J. Chem. Phys.* **152**, 234110 (2020). URL <https://doi.org/10.1063/5.0010549>.
- [33] Pal, A. Diffusion in a potential landscape with stochastic resetting. *Phys. Rev. E* **91**, 012113 (2015). URL <https://link.aps.org/doi/10.1103/PhysRevE.91.012113>.
- [34] Ray, S. Space-dependent diffusion with stochastic resetting: A first-passage study. *J. Chem. Phys.* **153**, 234904 (2020). URL <https://doi.org/10.1063/5.0034432>.
- [35] Sandev, T., Domazetoski, V., Kocarev, L., Metzler, R. & Chechkin, A. Heterogeneous diffusion with stochastic resetting. *J. Phys. A: Math. Theor.* **55**, 074003 (2022). URL <https://dx.doi.org/10.1088/1751-8121/ac491c>.
- [36] Stojkoski, V., Sandev, T., Kocarev, L. & Pal, A. Geometric Brownian motion under stochastic resetting: A stationary yet nonergodic process. *Phys. Rev. E* **104**, 014121 (2021). URL <https://link.aps.org/doi/10.1103/PhysRevE.104.014121>.
- [37] Evans, M. R. & Majumdar, S. N. Diffusion with resetting in arbitrary spatial dimension. *J. Phys. A: Math. Theor.* **47**, 285001 (2014). URL <https://dx.doi.org/10.1088/1751-8113/47/28/285001>.
- [38] Roldán, E. & Gupta, S. Path-integral formalism for stochastic resetting: Exactly solved examples and shortcuts to confinement. *Phys. Rev. E* **96**, 022130 (2017). URL <https://link.aps.org/doi/10.1103/PhysRevE.96.022130>.
- [39] Pinsky, R. G. Diffusive search with spatially dependent resetting. *Stoch. Process. Their Appl.* **130**, 2954–2973 (2020). URL <https://www.sciencedirect.com/science/article/pii/S0304414918302928>.
- [40] Vinod, D., Cherstvy, A. G., Wang, W., Metzler, R. & Sokolov, I. M. Nonergodicity of reset geometric Brownian motion. *Phys. Rev. E* **105**, L012106 (2022). URL <https://link.aps.org/doi/10.1103/PhysRevE.105.L012106>.
- [41] Vinod, D., Cherstvy, A. G., Metzler, R. & Sokolov, I. M. Time-averaging and nonergodicity of reset geometric Brownian motion with drift. *Phys. Rev. E* **106**, 034137 (2022). URL <https://link.aps.org/doi/10.1103/PhysRevE.106.034137>.
- [42] Wang, W., Cherstvy, A. G., Kantz, H., Metzler, R. & Sokolov, I. M. Time averaging and emerging nonergodicity upon resetting of fractional Brownian motion and heterogeneous diffusion processes. *Phys. Rev. E* **104**, 024105 (2021). URL <https://link.aps.org/doi/10.1103/PhysRevE.104.024105>.
- [43] Roldán, E., Lisica, A., Sánchez-Taltavull, D. & Grill, S. W. Stochastic resetting in backtrack recovery by RNA polymerases. *Phys. Rev. E* **93**, 062411 (2016). URL <https://link.aps.org/doi/10.1103/PhysRevE.93.062411>.
- [44] Tal-Friedman, O., Pal, A., Sekhon, A., Reuveni, S. & Roichman, Y. Experimental Realization of Diffusion with Stochastic Resetting. *J. Phys. Chem. Lett.* **11**, 7350–7355 (2020). URL <https://doi.org/10.1021/acs.jpcclett.0c02122>.
- [45] Robin, T., Reuveni, S. & Urbakh, M. Single-molecule theory of enzymatic inhibition. *Nat. Commun.* **9**, 779 (2018). URL <https://www.nature.com/articles/s41467-018-02995-6>.
- [46] Cherstvy, A. G., Kolomeisky, A. B. & Kornyshev, A. A. Protein-DNA Interactions: Reaching and Recognizing the Targets. *J. Phys. Chem. B* **112**, 4741–4750 (2008). URL <https://doi.org/10.1021/jp076432e>.
- [47] Weaver, D. *et al.* Distribution and Apoptotic Function of Outer Membrane Proteins Depend on Mitochondrial Fusion. *Mol. Cell.* **54**, 870–878 (2014). URL [https://www.cell.com/molecular-cell/abstract/S1097-2765\(14\)00317-7](https://www.cell.com/molecular-cell/abstract/S1097-2765(14)00317-7).
- [48] Taresté, D. & Roux, A. Common Energetic and Mechanical Features of Membrane Fusion and Fission Machineries. In Bassereau, P. & Sens, P. (eds.) *Physics of Biological Membranes*, 421–469 (Springer International Publishing, Cham, 2018). URL [https://doi.org/10.1007/978-3-030-00630-3\\_16](https://doi.org/10.1007/978-3-030-00630-3_16).
- [49] Saffi, G. T. & Botelho, R. J. Lysosome Fission: Planning for an Exit. *Trends Cell Biol.* **29**, 635–646 (2019). URL [https://www.cell.com/trends/cell-biology/abstract/S0962-8924\(19\)30082-0](https://www.cell.com/trends/cell-biology/abstract/S0962-8924(19)30082-0).
- [50] Dellaire, G., Ching, R. W., Dehghani, H., Ren, Y. & Bazett-Jones, D. P. The number of PML nuclear bodies

- increases in early S phase by a fission mechanism. *J. Cell Sci.* **119**, 1026–1033 (2006). URL <https://doi.org/10.1242/jcs.02816>.
- [51] Klosin, A. & Hyman, A. A. A liquid reservoir for silent chromatin. *Nature* **547**, 168–169 (2017). URL <https://www.nature.com/articles/nature23089>.
- [52] Bruens, L., Ellenbroek, S. I. J., van Rheeën, J. & Snippert, H. J. In Vivo Imaging Reveals Existence of Crypt Fission and Fusion in Adult Mouse Intestine. *Gastroenterology* **153**, 674–677.e3 (2017). URL <https://www.sciencedirect.com/science/article/pii/S0016508517356317>.
- [53] Samuk, K., Manzano-Winkler, B., Ritz, K. R. & Noor, M. A. F. Natural Selection Shapes Variation in Genome-wide Recombination Rate in *Drosophila pseudoobscura*. *Curr. Biol.* **30**, 1517–1528.e6 (2020). URL <https://www.sciencedirect.com/science/article/pii/S0960982220304231>.
- [54] Peñalba, J. V. & Wolf, J. B. W. From molecules to populations: appreciating and estimating recombination rate variation. *Nat. Rev. Genet.* **21**, 476–492 (2020). URL <https://www.nature.com/articles/s41576-020-0240-1>.
- [55] Cremer, J., Melbinger, A. & Frey, E. Growth dynamics and the evolution of cooperation in microbial populations. *Sci. Rep.* **2**, 281 (2012). URL <https://www.nature.com/articles/srep00281>.
- [56] Rulands, S. *et al.* Universality of clone dynamics during tissue development. *Nature Phys.* **14**, 469–474 (2018). URL <https://www.nature.com/articles/s41567-018-0055-6>.
- [57] Zwicker, D., Seyboldt, R., Weber, C. A., Hyman, A. A. & Jülicher, F. Growth and division of active droplets provides a model for protocells. *Nature Phys.* **13**, 408–413 (2017). URL <https://www.nature.com/articles/nphys3984>.
- [58] Slootbeek, A. D., Haren, M. H. I. v., Smokers, I. B. A. & Spruijt, E. Growth, replication and division enable evolution of coacervate protocells. *Chem. Commun.* **58**, 11183–11200 (2022). URL <https://pubs.rsc.org/en/content/articlelanding/2022/cc/d2cc03541c>.
- [59] Anderson, P. W. Absence of Diffusion in Certain Random Lattices. *Phys. Rev.* **109**, 1492–1505 (1958). URL <https://link.aps.org/doi/10.1103/PhysRev.109.1492>.
- [60] Evans, M. R., Majumdar, S. N. & Schehr, G. Stochastic resetting and applications. *J. Phys. A: Math. Theor.* **53**, 193001 (2020). URL <https://dx.doi.org/10.1088/1751-8121/ab7cfe>.
- [61] This applies particularly for three-dimensional systems, to which our results straight-forwardly extend.
- [62] Chagnon, P.-L. Ecological and evolutionary implications of hyphal anastomosis in arbuscular mycorrhizal fungi. *FEMS Microbiology Ecology* **88**, 437–444 (2014). URL <https://doi.org/10.1111/1574-6941.12321>.
- [63] Marleau, J., Dalpé, Y., St-Arnaud, M. & Hijri, M. Spore development and nuclear inheritance in arbuscular mycorrhizal fungi. *BMC Evolutionary Biology* **11**, 51 (2011). URL <https://doi.org/10.1186/1471-2148-11-51>.
- [64] de Novais, C. B., Sbrana, C., Júnior, O. J. S., Siqueira, J. O. & Giovannetti, M. Vegetative compatibility and anastomosis formation within and among individual germings of tropical isolates of arbuscular mycorrhizal fungi (Glomeromycota). *Mycorrhiza* **23**, 325–331 (2013). URL <https://doi.org/10.1007/s00572-013-0478-y>.
- [65] Gabriela Roca, M., Read, N. D. & Wheals, A. E. Conidial anastomosis tubes in filamentous fungi. *FEMS Microbiology Letters* **249**, 191–198 (2005). URL <https://doi.org/10.1016/j.femsle.2005.06.048>.
- [66] Mayers, C. G., Harrington, T. C., Wai, A. & Hausner, G. Recent and Ongoing Horizontal Transfer of Mitochondrial Introns Between Two Fungal Tree Pathogens. *Front. Microbiol.* **12** (2021). URL <https://www.frontiersin.org/journals/microbiology/articles/10.3389/fmicb.2021.656609/full>. Publisher: Frontiers.
- [67] Martinez, L. M. & Viegas, J. M. Assessing the impacts of deploying a shared self-driving urban mobility system: An agent-based model applied to the city of Lisbon, Portugal. *International Journal of Transportation Science and Technology* **6**, 13–27 (2017). URL <https://www.sciencedirect.com/science/article/pii/S2046043016300442>.
- [68] Boeing, G. OSMnx Paper (2024). URL <https://geoffboeing.com/publications/osmnx-paper/>.
- [69] Bruggeman, J., Sprik, R. & Quax, R. Spontaneous cooperation for public goods. *J. Math. Sociol.* **45**, 183–191 (2021). URL <https://doi.org/10.1080/0022250X.2020.1756285>.
- [70] Dutta, J. & Michel, P. The Distribution of Wealth with Imperfect Altruism. *J. Econ. Theory* **82**, 379–404 (1998). URL <https://www.sciencedirect.com/science/article/pii/S002205319792442X>.

### Appendix A: Definition of the Resetting and the Diffusion operator

As introduced above, we consider  $N$  particles described by their positions  $X_i \in \mathbb{R}$  in one spatial dimension, which undergo Brownian motion with diffusion constant  $D$  and which are subject to cooperative resetting dynamics. To describe the collective behavior of this system, we study the single-particle probability density,  $p(x, t)$ . The time evolution of  $p(x, t)$  is governed by two processes: the effect of Brownian motion, which depends on the single-particle density  $p(x, t)$ , and the pair-wise resetting, which depends on the two-particle density  $p_2(x, x', t)$ . We define the diffusion operator at position  $\tilde{x}$  as

$$\hat{\mathcal{L}}[p(x, t)]\Big|_{x=\tilde{x}} = D \frac{\partial^2}{\partial x^2} p(\tilde{x}, t) \quad (\text{A1})$$

which is the standard expression for the diffusion flux. For the resetting operator, we compute the rate of a particle being *added* at position  $\tilde{x}$  and subtract the rate of a particle being *removed* at position  $\tilde{x}$  due to cooperative resetting,

$$\begin{aligned} \hat{\mathcal{R}}[p_2(x, x', t)]\Big|_{x=\tilde{x}} &= \frac{1}{2} \int_{-\infty}^{\infty} \int_{-\infty}^{\infty} dx dx' p_2(x, x', t) \mu(x - x') \delta\left(\tilde{x} - \frac{x + x'}{2}\right) \\ &\quad - \int_{-\infty}^{\infty} dx' p_2(\tilde{x}, x', t) \mu(\tilde{x} - x'). \end{aligned} \quad (\text{A2})$$

### Appendix B: Flux Formulation of the Resetting and the Diffusion operator

Accounting for the fact that resetting conserves the total number of particles, instead of referring to source and sink terms, we consider the displacement of particles. This allows us to rephrase the resetting operator as a derivative of a flux

$$\hat{\mathcal{R}}[p_2(x, x', t)]\Big|_{x=\tilde{x}} = - \frac{\partial}{\partial x} \hat{J}_{\mathcal{R}}[p_2(x, x', t)]\Big|_{x=\tilde{x}} \quad (\text{B1})$$

where the flux is

$$\hat{J}_{\mathcal{R}}[p_2(x, x', t)]\Big|_{x=\tilde{x}} = \frac{1}{2} \int_{-\infty}^{\infty} \int_{-\infty}^{\infty} dx dx' p_2(x, x', t) \mu(x - x') \Theta((x - \tilde{x})(\tilde{x} - x)) \operatorname{sgn}\left(\frac{x + x'}{2} - \tilde{x}\right). \quad (\text{B2})$$

Analogously, the diffusion processes can be rephrased as the derivative of a diffusion flux, where the diffusion flux is

$$\hat{J}_{\mathcal{L}}[p(x, t)]\Big|_{x=\tilde{x}} = -D \frac{\partial}{\partial x} p(x, t). \quad (\text{B3})$$

### Appendix C: Approximation of the resetting flux

We approximate the resetting flux by making use of a mean-field approximation such that  $p_2(x, x', t) = p(x, t)p(x', t)$ . We define two integration sets by making the definition of the sign function explicit,

$$\begin{aligned} I_+(\tilde{x}) &= \left\{ (x, x') \mid x < \tilde{x} \wedge \frac{x' + x}{2} > \tilde{x} \right\} \\ I_-(\tilde{x}) &= \left\{ (x, x') \mid x > \tilde{x} \wedge \frac{x' + x}{2} < \tilde{x} \right\}. \end{aligned} \quad (\text{C1})$$

Furthermore, we perform a transformation to spherical coordinates, such that

$$\begin{aligned} x &= \cos(\theta)r + \tilde{x} \\ x' &= \sin(\theta)r + \tilde{x}. \end{aligned} \quad (\text{C2})$$

The double integral then simplifies to

$$\hat{J}_{\mathcal{L}}[p(x, t)] \Big|_{x=\tilde{x}} = \int_{\pi/2}^{3\pi/4} \frac{3\pi}{4} d\theta \int_0^\infty dr r \mu(r(\cos(\theta) - \sin(\theta))) [f(\cos(\theta)r + \tilde{x})f(\sin(\theta)r + \tilde{x}) - f(-\cos(\theta)r + \tilde{x})f(-\sin(\theta)r + \tilde{x})]. \quad (\text{C3})$$

We find that this transformation allows to extract the intrinsic symmetries of the integral. We define

$$g(r, \theta, \tilde{x}, t) = \mu(r(\cos(\theta) - \sin(\theta))) (p(\cos(\theta)r + \tilde{x})p(\sin(\theta)r + \tilde{x}) - p(-\cos(\theta)r + \tilde{x})p(-\sin(\theta)r + \tilde{x})), \quad (\text{C4})$$

$$(\text{C5})$$

as the integrand. The line integral vanishes along the axis  $\theta = 3\pi/4$  by construction. Furthermore, the line integral  $\int_0^\infty dr g(r, \theta, \tilde{x}, t)$  is maximal along the axis  $\theta = \pi/2$  and decays monotonically in  $\theta \in [\pi/2, 3\pi/4]$  if  $p(x + x', t)^2 > p(x, t)p(x + 2x', t)$  for all  $x, x' \in \mathbb{R}$ .

We next perform a first-order expansion over the arc integral as we take the limit  $r \rightarrow \infty$ , which can be visualized as a triangulation of the integral. We find that the arc integral is approximated by

$$I_\theta(r, \tilde{x}, t) = \frac{1}{2} \mu(r) \left| \frac{p(\tilde{x}, t)}{rp'(\tilde{x}, t)} \right| [p(\tilde{x} + r, t) - p(\tilde{x} - r, t)] + \mathcal{O}(r^{-2}). \quad (\text{C6})$$

The integral can be read as the area of a triangle of height  $h = p(\tilde{x} + r, t)$  and base  $\mu(r) \left| \frac{p(\tilde{x}, t)}{rp'(\tilde{x}, t)} \right|$ . Here, we find how the inverse normalized gradient arises from a linearization at  $\theta = \pi/2$  along the arc and solving a function of the form  $0 = m + b\theta$ , where  $b$  is the gradient.

Next, we account for the radial integration and the back transformation of the variables. To this end, we find that the approximation of the arc integral to first order in  $1/r$  is admissible if we consider the flux in the tail of  $p(x)$ , which is equivalent to taking the limit  $|x| \rightarrow \infty$ . With this, we find that the double integral simplifies to

$$\hat{J}_{\mathcal{R}}[p_2(x, x', t)] \Big|_{x=\tilde{x}} \approx \frac{1}{2} \frac{\mu_0}{|\tilde{x}|^\alpha} p(\tilde{x}) \left| \frac{p(\tilde{x})}{p'(\tilde{x})} \right|. \quad (\text{C7})$$

#### Appendix D: Higher-order approximation for algebraically decaying probability densities

From Eq. (4) we find that for quadratically decaying resetting interactions the steady state probability densities show an algebraic decay with  $p_s(\chi) \propto \chi^{-\sqrt{\varrho}}$  for  $|\chi| \rightarrow \infty$ . We validated this result for  $\varrho \gg 1$  numerically (Fig. 2b). Yet, the condition  $p(x + x', t)^2 > p(x, t)p(x + 2x', t)$  for all  $x, x' \in \mathbb{R}$  is not fulfilled for algebraically decaying probability distribution. As a consequence,  $g(r, \theta, \tilde{x}, t)$  is not granted to be a monotonic function on the interval  $\theta \in [\pi/2, 3\pi/4]$ . In particular in the region, where the probability distribution can be well approximated by an algebraic decay,  $g(r, \theta, \tilde{x}, t)$  obtains both negative and positive values. Nonetheless, the approximation in Appendix C still works well for the region close to the center of the distribution around  $x_0$ , which is dominating the resetting flux.

To refine the approximation in Appendix C, we define two regions. Given the interaction length scale  $\delta_0$ , we define a region  $[x_0 - 2\delta_0, x_0 + 2\delta_0]$  as the center of the distribution and the remaining parts of the distribution as the tail region of the distribution. We find that due to the non-monotonicity of  $p(x) \propto x^{-a}$  the region  $r > \tilde{x} + 2\delta_0$  is inflicted with negative values of  $g(r, \theta, \tilde{x}, t)$  in the interval  $\theta \in [\pi/2, 3\pi/4]$ . Here, we defined the exponent of the decaying probability distribution to be  $a$ . Effectively, the arc integral  $I_\theta(r, \tilde{x}, t)$  vanishes in the tail region. We account for this by employing a factor  $\Lambda(a) = 1 - \int_{2\delta}^\infty dx p(x) - \int_{-\infty}^{-2\delta}$  which modifies equation Eq. (4) as

$$\varrho \Lambda(a) p_s(\chi) \left| \frac{p_s(\chi)}{p'_s(\chi)} \right| |\chi|^{-\alpha} \stackrel{!}{=} p'_s(\chi). \quad (\text{D1})$$

As a consequence, the steady state probability distribution needs to solve the equation  $\varrho \Lambda(a) = a^2$ . We find that  $\Lambda(a)$  is well approximated by the analytical function  $\Lambda(a) \approx 1 - (2^{(1-a)} a \sin(\pi/a)) / ((-1 + a)\pi)$ . Making use of this function, we find that the consistency equation only yields solutions  $a(\varrho)$  if  $\sqrt{\varrho} > 2.3$ . This gives a refined approximation for the critical rescaled density in line with the numerical observation in Fig. 2d.



### Appendix E: Numerical Simulations

For the numerical validation backing our general analytical findings, we performed agent-based simulations. For the Brownian motion, we perform independent simulations of particles by the numerical integration of stochastic differential equations. This yields a set of stochastic realizations. To implement resetting, at each time step, we compute the rate of each pair of particles to reset to their respective mean position. Based on this rate, we update two randomly chosen particles by setting them to their mean positions using a stochastic simulation algorithm. In between resetting events, the particles again independently perform Brownian motion.